

Experimental observation of the role of counteranions on the electrical conductance of Preyssler-type polyoxometalate nanodevices.

Cécile Huez,^{1,‡} Séverine Renaudineau,² Florence Volatron,²
Anna Proust² and Dominique Vuillaume.¹

*1) Institute for Electronics Microelectronics and Nanotechnology (IEMN), CNRS,
University of Lille, Av. Poincaré, Villeneuve d'Ascq, France*

*2) Institut Parisien de Chimie Moléculaire (IPCM), CNRS, Sorbonne Université,
4 Place Jussieu, Paris, France*

‡) Now at : Instituto de Ciencia Molecular (ICMoL), University of Valencia, Spain.

SUPPORTING INFORMATION

1. Synthesis Details

All the chemicals were used as supplied. $K_{12,5}Na_{1,5}[NaCP_5W_{30}O_{110}]$,¹ $(NH_4)_{14}[NaCP_5W_{30}O_{110}]$,² and $H_{14}[NaCP_5W_{30}O_{110}]$,³ were prepared according to published procedures and their purity checked by IR and ³¹P NMR spectroscopy. The synthesis of $TBA_{10}H_4[NaCP_5W_{30}O_{110}]$ was adapted from the literature.⁴ IR spectra (KBr pellets) have been recorded in transmission from 250 to 4000 cm^{-1} on a Jasco FT/IR 4100 spectrometer (Resolution 4 cm^{-1}). ³¹P NMR spectra (121 MHz) have been recorded on a Bruker Avance II 300MHz spectrometer and the chemical shifts referenced to external 85 % H_3PO_4 . Thermogravimetric

analyses (TGA) have been performed on SDT-Q600 TA Instrument thermobalance under an air flow to assess the amount of water molecules. Elemental analyses have been carried out at Crealins and at the Institut des Sciences Analytiques, CNRS, Villeurbanne, France.

Synthesis and characterization of $K_{12,5}Na_{1,5}[Na\subset P_5W_{30}O_{110}]$

To 33g of $Na_2WO_4 \cdot 2H_2O$ dissolved in 30mL of water were added 26.5mL of H_3PO_4 (85%). This mixture was placed in a solvothermal synthesis bomb (Parr Model 4748), heated to 120°C overnight. Once the yellow solution has been cooled to room temperature, 15mL of H_2O was added followed by 10g of KCl. The precipitate was membrane filtered and washed with 2M potassium acetate and methanol. Recrystallization in hot water was necessary to purify the product (with a pause time < 2h to avoid the formation of crystals of $[a-P_2W_{18}O_{62}]^{6-}$). About 8g of crystals are then collected (yield about 30%). A second recrystallization can be performed if the product still contains impurities. For each step, the purity was assessed by ^{31}P NMR: the small signal at -12,55 ppm corresponds to $[a-P_2W_{18}O_{62}]^{6-}$.⁵ Thermogravimetric analysis gave 27 water molecules of crystallization.

IR (KBr, cm^{-1}): n 3538 (m), 3432 (m), 1616 (m), 1164 (m), 1082 (m), 1017 (w), 982 (sh), 936 (s), 911 (s), 782 (s), 670 (sh), 571 (w), 538 (w), 464 (w), 349 (m), 311 (w), 286 (w). ^{31}P NMR (D_2O): $\delta = -9.61$ ppm. Elemental analysis: found (calculated for $K_{13,3}Na_{0,7}[Na\subset P_5W_{30}O_{110}] \cdot 27H_2O$ MW = 8475.07 g mol⁻¹) K: 6.12 (6.14), Na: 0.42 (0.46), P: 1.76 (1.83), W: 65.23 (65.08) %.

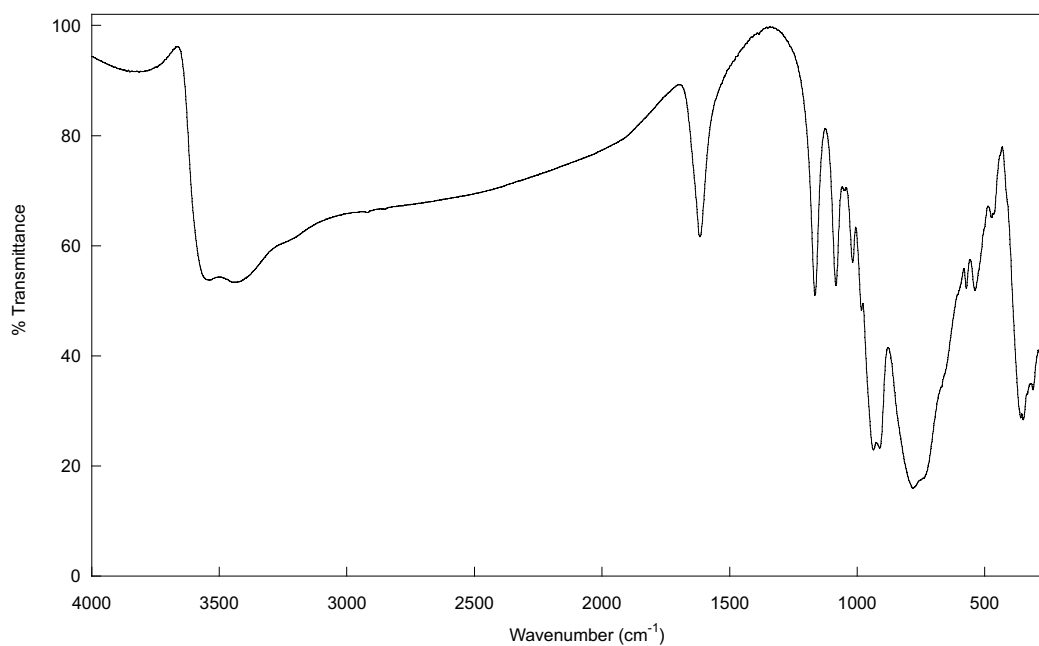


Figure S1. IR spectrum of $K_{13,3}Na_{0,7}[NaCP_5W_{30}O_{110}]$ (KBr pellet).

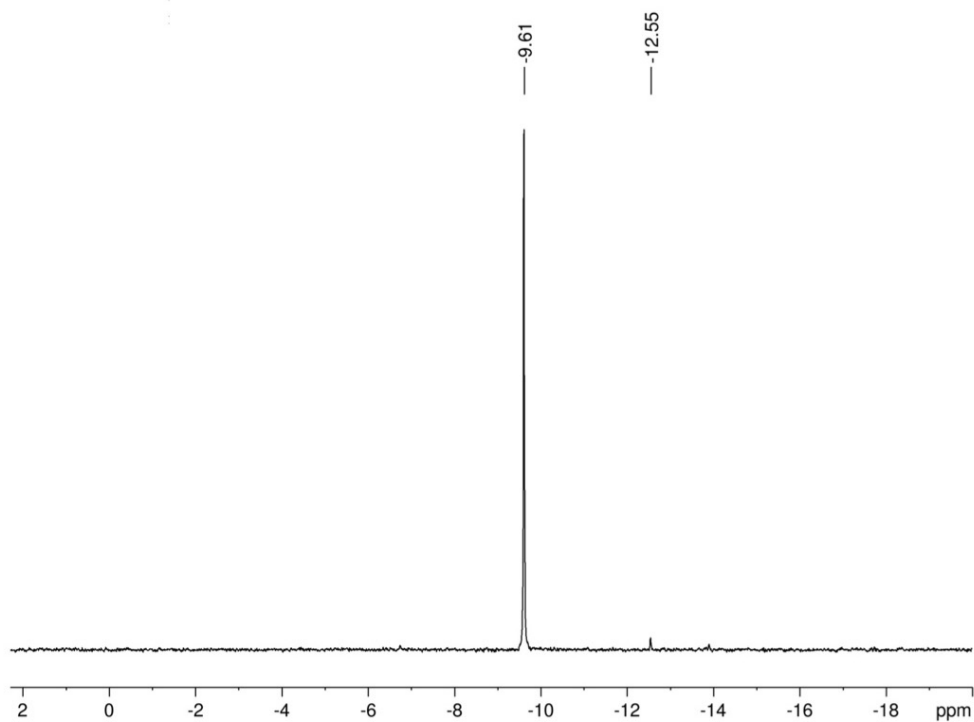


Figure S2. ^{31}P NMR spectrum of $K_{13,3}Na_{0,7}[NaCP_5W_{30}O_{110}]$ in D_2O .

Synthesis of $(\text{NH}_4)_{14}[\text{Na}_5\text{P}_5\text{W}_{30}\text{O}_{110}]$

The synthesis was performed following the published procedure and thermogravimetric analysis carried out on an air-dried sample gave 25 water molecules of crystallization.

IR (KBr, cm^{-1}): n 3551 (m), 3443 (m), 3127 (m), 1615 (m), 1400 (s), 1165 (m), 1080 (m), 1017 (m), 982 (w), 934 (s), 910 (s), 777 (s), 571 (w), 539 (w), 470 (w), 359 (m), 311 (w). ^{31}P NMR (D_2O): $\delta = -9.61$ ppm.

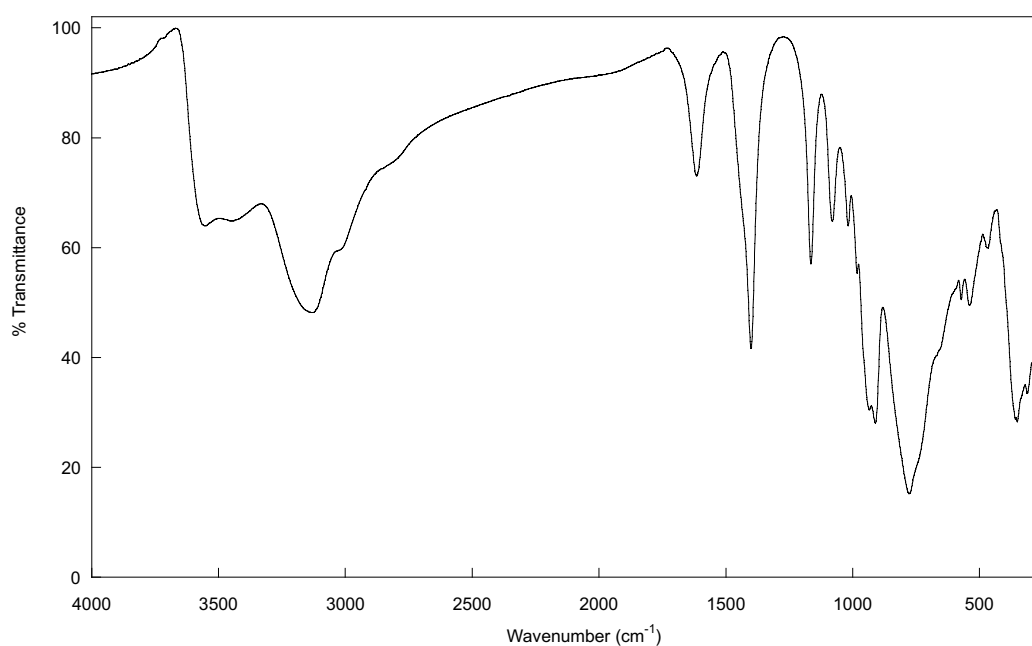


Figure S3. IR spectrum of $(\text{NH}_4)_{14}[\text{Na}_5\text{P}_5\text{W}_{30}\text{O}_{110}]$ (KBr pellet).

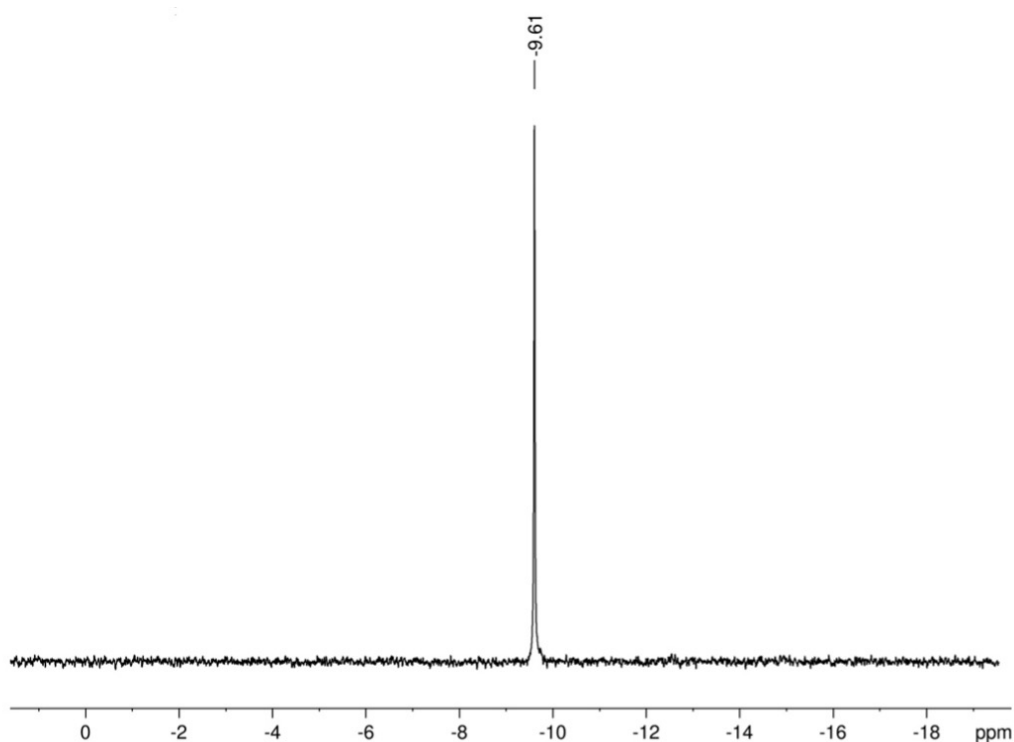


Figure S4. ^{31}P NMR spectrum of $(\text{NH}_4)_{14}[\text{NaC}_5\text{P}_5\text{W}_{30}\text{O}_{110}]$ in D_2O .

Synthesis of $\text{H}_{14}[\text{NaC}_5\text{P}_5\text{W}_{30}\text{O}_{110}]$

First, we prepared the Dowex column 50W-X8 in its acidic form. In a beaker, the very fine particles of the resin were separated from the mass by successive sedimentations and settlings in distilled water. The resin was then washed with distilled water until the orange coloration resulting from the degradation of the polymer disappeared. Finally, the resin was placed in a column (diameter 1.5 cm, length 40 cm), washed three times with its dead volume of 1M HCl (~3x20 mL) and rinsed with water until the pH obtained for the eluent reached that of distilled water.⁶ In a second step, 8.2g of $\text{K}_{13,3}\text{Na}_{0,7}[\text{NaC}_5\text{P}_5\text{W}_{30}\text{O}_{110}]\cdot 27\text{H}_2\text{O}$ were dissolved in 160 mL of H_2O . The solution was transferred to the column and passed through the resin at a rate of one drop per second. Water (~40mL) was then passed through the column, as long as the pH of the eluent remained acidic to ensure that all the product was collected. The eluent was then evaporated at a

temperature of 60-65°C to recover the product as a yellow and sticky solid, which was crushed twice with ethanol, then dried with diethylether (yield 7.8g). According to thermogravimetric analysis, 44 water molecules are present leading to the general formula $H_{14}[NaCP_5W_{30}O_{110}].44H_2O$.

IR (KBr, cm^{-1}): n 3400 (m), 3199 (w), 1708 (w), 1624 (m), 1604 (m), 1163 (m), 1080 (m), 1022 (m), 939 (s), 914 (s), 765 (s), 670 (sh), 571 (w), 532 (w), 465 (w), 355 (m), 342 (m), 301 (w). ^{31}P NMR (D_2O): $\delta = -9.61$ ppm. Elemental analysis: found (calculated for $H_{14}[NaCP_5W_{30}O_{110}].44H_2O$ $M = 8260.08$ g mol^{-1}) H: 1.47 (1.24), Na: 0.38 (0.28), P: 1.68 (1.87), W: 66.34 (66.77) %.

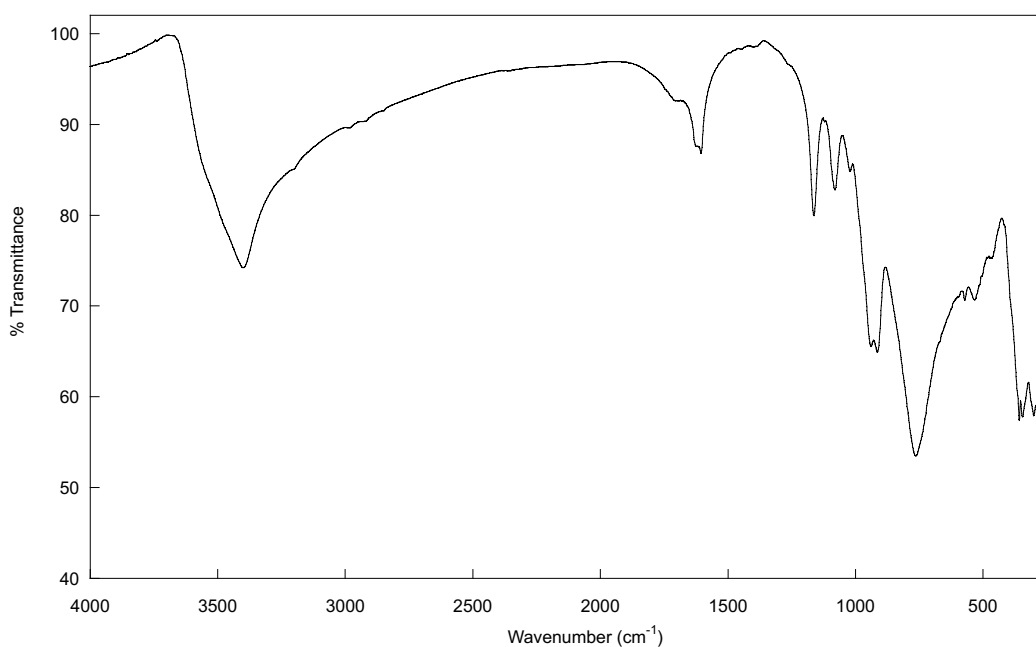


Figure S5. IR spectrum of $H_{14}[NaCP_5W_{30}O_{110}]$ (KBr pellet).

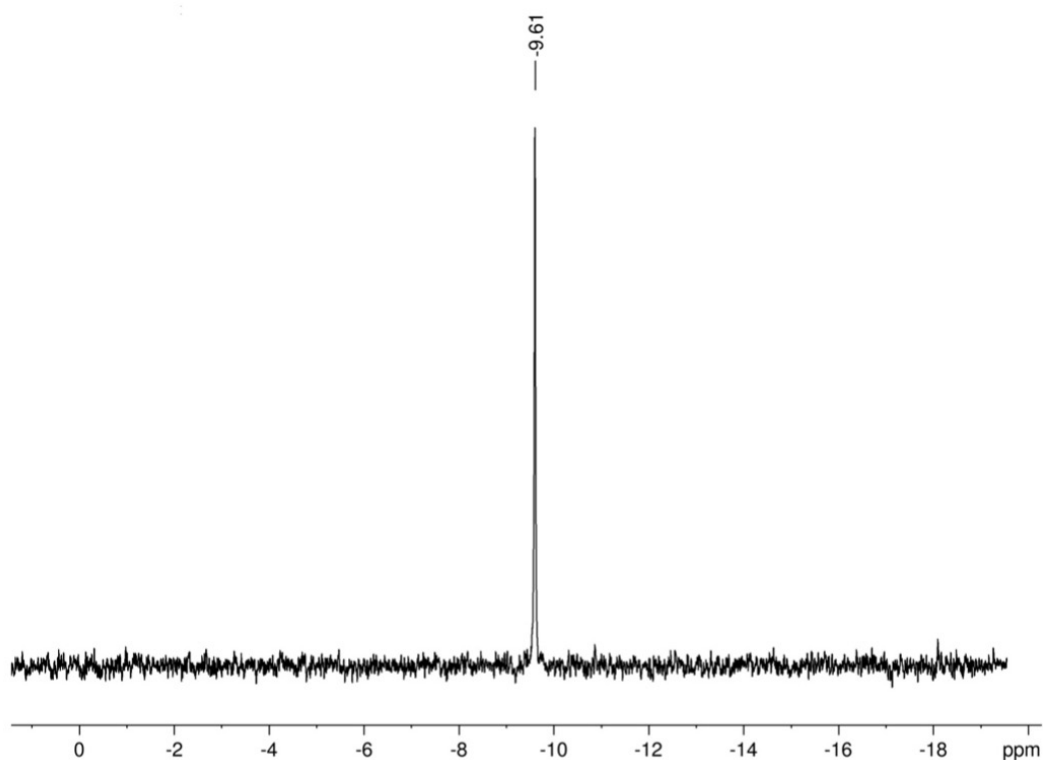


Figure S6. ^{31}P NMR spectrum of $\text{H}_{14}[\text{NaCP}_5\text{W}_{30}\text{O}_{110}]$ in D_2O .

Synthesis of $\text{TBA}_{10}\text{H}_4[\text{NaCP}_5\text{W}_{30}\text{O}_{110}]$ adapted from reference 3.

In a bicol flask, 6.0 g (0.73 mmole) of $\text{H}_{14}[\text{NaCP}_5\text{W}_{30}\text{O}_{110}]\cdot 44\text{H}_2\text{O}$ were dissolved in 100 mL of degassed distilled water, 2 drops of phenolphthalein were added to clearly see the turning point. The solution was titrated with a 1.54 M TBAOH solution (40 wt% in water, independently titrated) and the titration was monitored with a pH electrode under a nitrogen flow. The TBAOH solution was added slowly with a syringe, the solution became milky very quickly but cleared again shortly before the turning point. After addition of 4.8 mL of the 1.54 M TBAOH solution plus 0.1 mL of a 5-fold diluted (0.308 M) TBAOH solution, the solution remained slightly pinkish. It was then evaporated under vacuum. During the evaporation, a fading of the solution was observed which showed that the pH slightly decreased, the evaporation was stopped for addition of a small amount of the TBAOH solution. The phenomenon was repeated 3 times bringing the

equivalent number of TBAOH to 7.70 mmoles (instead of the 10.22 mmoles expected for titration of the 14 protons per polyoxometalate). The product was dried with 2x10 mL absolute ethanol and 10 mL ether. The presence of 24 water molecules was determined by thermogravimetric analysis, leading to the formula $\text{TBA}_{10}\text{H}_4[\text{Na}\text{C}\text{P}_5\text{W}_{30}\text{O}_{110}]\cdot 24\text{H}_2\text{O}$.

IR (KBr, cm^{-1}): ν 3407 (m), 2960 (m), 2933 (w), 2871 (m), 2741 (w), 1636 (m), 1484 (m), 1380 (w), 1160 (m), 1075 (m), 1018 (m), 982 (m), 918 (s), 794 (s), 747 (s), 573 (w), 541 (w), 474 (w), 369 (m), 312 (m). ^{31}P NMR (CD_3CN) δ = -9.06 ppm. Elemental analysis: found (calculated for $\text{TBA}_{10}\text{H}_4[\text{Na}\text{C}\text{P}_5\text{W}_{30}\text{O}_{110}]\cdot 24\text{H}_2\text{O}$ MW = 10314.41 $\text{g}\cdot\text{mol}^{-1}$) C: 19.26 (18.63) H: 3.96 (4.03), N: 1.45 (1.36); Na: 0.32 (0.22), P: 0.91 (1.50), W: 52.66 (53.47)%.

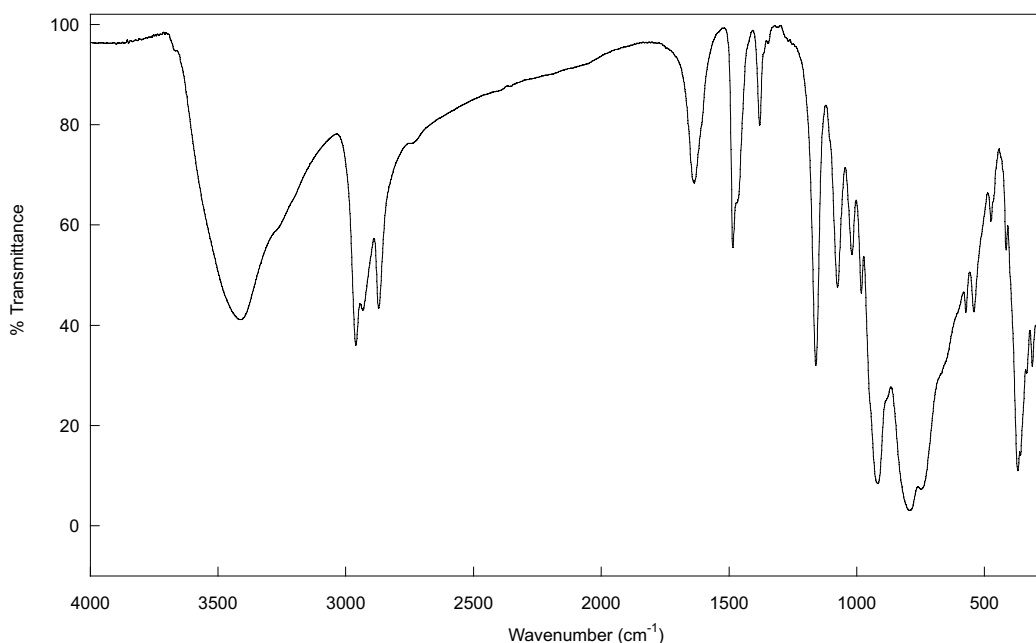


Figure S7. IR spectrum of $\text{TBA}_{10}\text{H}_4[\text{Na}\text{C}\text{P}_5\text{W}_{30}\text{O}_{110}]$ (KBr pellet).

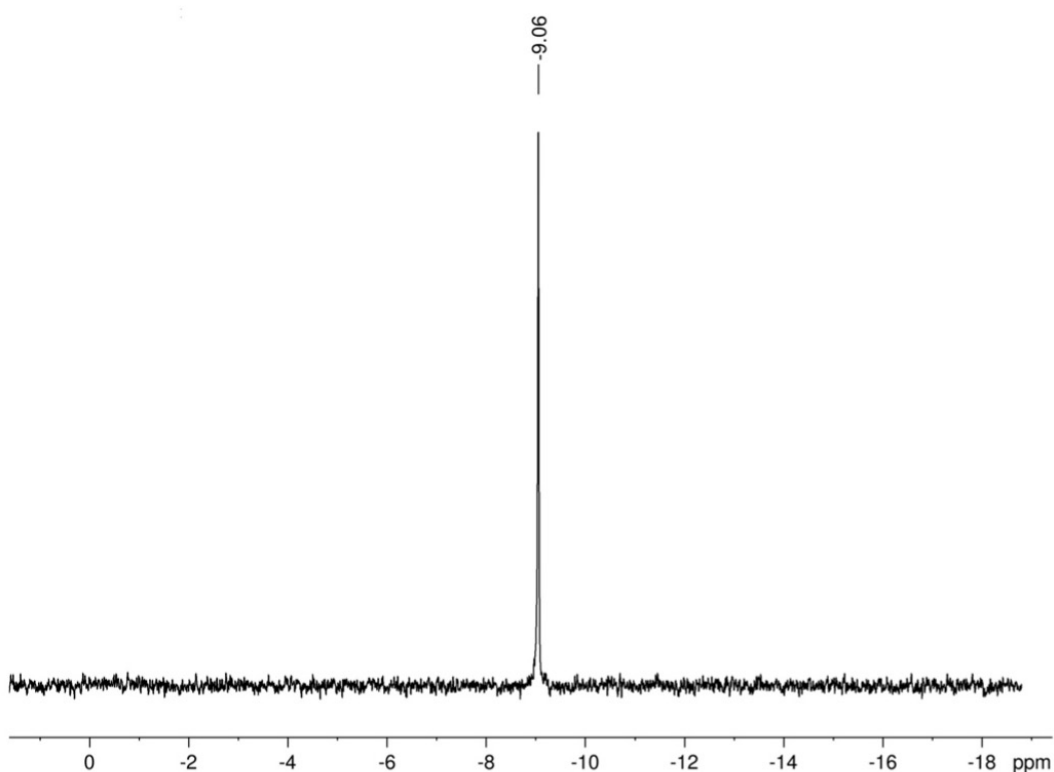


Figure S8. ^{31}P NMR spectrum of $\text{TBA}_{10}\text{H}_4[\text{NaC}_5\text{P}_5\text{W}_{30}\text{O}_{110}]$ in CD_3CN .

2. Self-Assembled Monolayer

Ultraflat template-stripped gold surfaces ($\text{T}^{\text{S}}\text{Au}$), with rms roughness of ~ 0.4 nm were prepared according to the method already reported.⁷⁻⁹ In brief, a 300–500 nm thick Au film was evaporated on a very flat silicon wafer covered by its native SiO_2 (rms roughness of ~ 0.4 nm), which was previously carefully cleaned by piranha solution (30 min in 7:3 $\text{H}_2\text{SO}_4/\text{H}_2\text{O}_2$ (v/v); **Caution:** Piranha solution is a strong oxidizer and reacts exothermically with organics), rinsed with deionized (DI) water, and dried under a stream of nitrogen. Clean 10x10 mm pieces of glass slide (ultrasonicated in acetone for 5 min, ultrasonicated in 2-propanol for 5 min, and UV irradiated in ozone for 10 min) were glued on the evaporated Au film (UV-polymerizable glue, NOA61 from Epotecnycy), then mechanically peeled off

providing the ^{TS}Au film attached on the glass side (Au film is cut with a razor blade around the glass piece).

The self-assembled monolayers (SAMs) of 6-aminohexane-1-thiol hydrochloride ($HS-(CH_2)_6-NH_3^+/Cl^-$) were prepared following a protocol optimized and described in a previous work for the electrostatic immobilization of POMs on amine-terminated SAMs.^{10, 11} The freshly prepared ^{TS}Au substrates were dipped in a solution of 6-aminohexane-1-thiol hydrochloride (Sigma-Aldrich) at a concentration of 10^{-3} M in ethanol overnight in the dark. The samples were rinsed in ethanol for 5 min and then ultrasonically cleaned 5 min in deionized (DI) water. These SAMs were treated by a PBS (phosphate-buffered saline, pH=7.4) solution for 2 hours, followed by ultra-sonication in DI water for 5 minutes. The substrates were finally washed with ethanol and dried under nitrogen flow. It was found that the PBS treatment removes the formation of aggregates on the aminoalkylthiol SAMs as well as avoids clustering of POMs during the electrostatic deposition, likely because this treatment optimizes the ratio of NH_3^+/NH_2 on the surface.¹⁰ The electrostatic deposition of the POMs was done by immersion of these SAMs in a solution of POM at a concentration of 10^{-3} M in H_2O , except for HP_5W_{30} and $TBAP_5W_{30}$ dissolved in ACN/isopropanol, for one to few hours. We checked by ellipsometry that the thickness of the POM layer was independent of the immersion time when the immersion time was longer than 1h.

3. Ellipsometry Measurements

We recorded spectroscopic ellipsometry data (on *ca.* 1 cm² samples) in the visible range using a UVISEL (Horiba Jobin Yvon) spectroscopic ellipsometer equipped with DeltaPsi 2 data analysis software. The system acquired a spectrum ranging from 2 to 4.5 eV (corresponding to 300–750 nm) with intervals of 0.1 eV (or 15 nm). The data were taken at an angle of incidence of 70°, and the compensator

was set at 45°. We fit the data by a regression analysis to a film-on-substrate model as described by their thickness and their complex refractive indexes. First, a background for the substrate before monolayer deposition was recorded. We acquired three reference spectra at three different places of the surface spaced of few mm. Secondly, after the monolayer deposition, we acquired once again three spectra at three different places of the surface and we used a 2-layer model (substrate/SAM) to fit the measured data and to determine the SAM thickness. We employed the previously measured optical properties of the substrate (background), and we fixed the refractive index of the monolayer at 1.50.¹² We note that a change from 1.50 to 1.55 would result in less than a 1 Å error for a thickness less than 30 Å. The three spectra measured on the sample were fitted separately using each of the three reference spectra, giving nine values for the SAM thickness. We calculated the mean value from this nine thickness values and the thickness incertitude corresponding to the standard deviation. Overall, we estimated the accuracy of the SAM thickness measurements at ± 2 Å.¹³

4. C-AFM Measurements

We measured the electron transport properties at the nanoscale by CAFM (ICON, Bruker) at room temperature using a tip probe in platinum/iridium. We used a "blind" mode to measure the current-voltage (I-V) curves and the current histograms: a square grid of 10×10 was defined with a pitch of 50 to 100 nm. At each point, the I-V curve is acquired leading to the measurements of 100 traces per grid. This process was repeated several times at different places (randomly chosen) on the sample, and up to several thousand of I-V traces were used to construct the current-voltage histograms (shown in Fig. 3, main text).

The tip load force was set at $\approx 6-9$ nN for all the I-V measurements, a lower value leading to too many contact instabilities during the I-V measurements. Albeit larger than the usual load force (2-5 nN) used for CAFM on SAMs, this value is

below the limit of about 60-70 nN at which the SAMs start to suffer from severe degradations. For example, a detailed study (Ref. 14) showed a limited strain-induced deformation of the monolayer (≈ 0.3 nm) at this used load force. The same conclusion was confirmed by our own study comparing mechanical and electrical properties of alkythiol SAMs on flat Au surfaces and tiny Au nanodots.¹⁵

5. Details of the I-V measurements

From the datasets shown in Fig. 2, we extracted the distribution of the current measured at +/- 0.5V (Fig. S9) and +/- 1V (Fig. S10) to support the results shown in Fig. 3b (evolution of the current with the nature of the counterions).

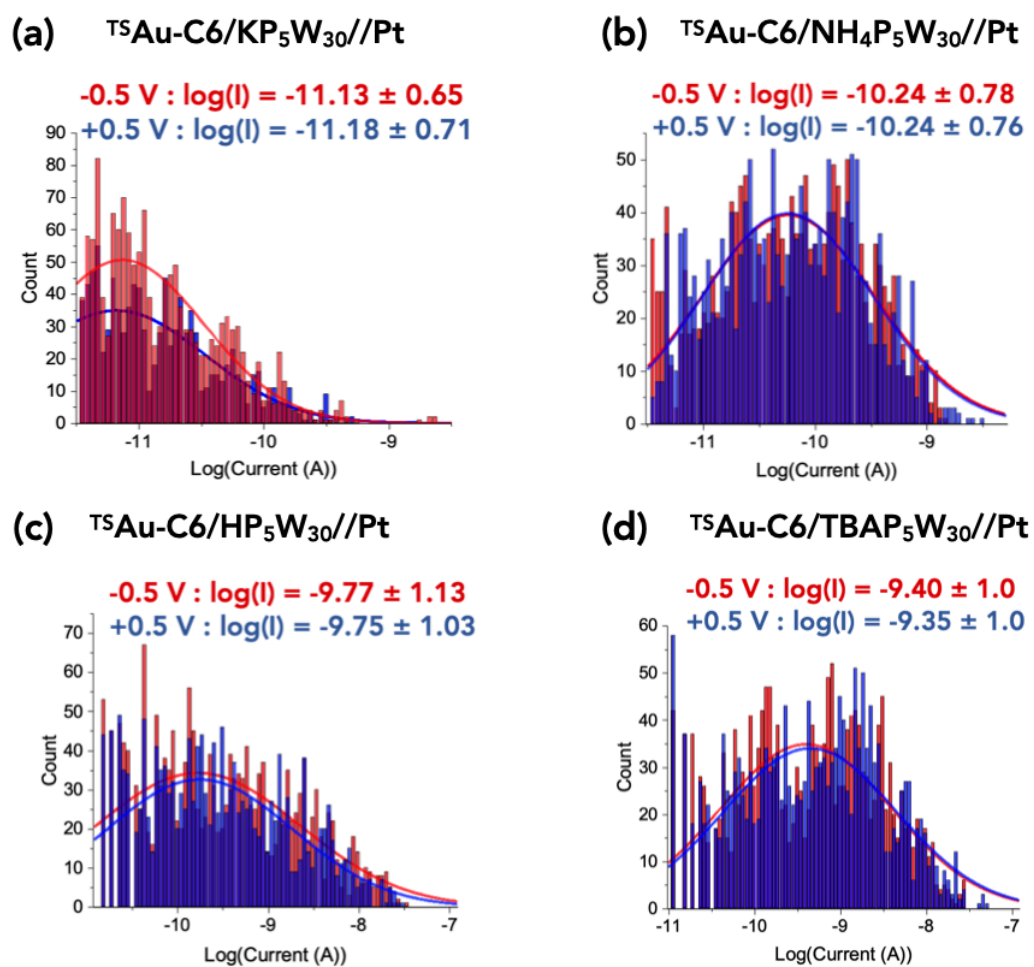
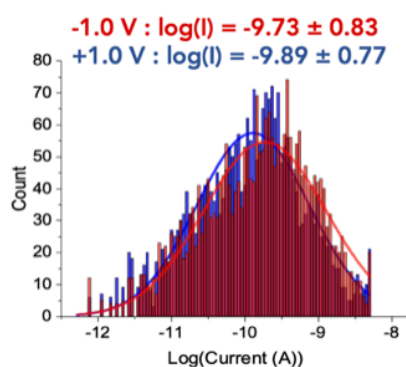
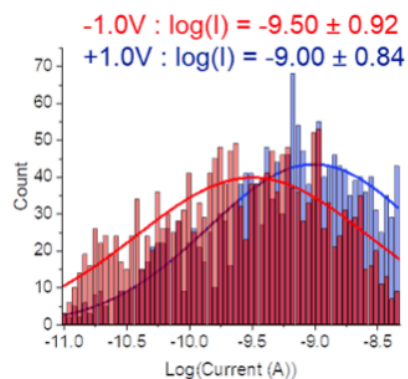


Figure S9. Histograms of $\log(\text{current})$ measured at 0.5V and -0.5V for the four samples. The solid lines are the fit by a log-normal distribution with the values of the log-mean ($\log(\bar{I})$) and a log standard deviation ($\log(\sigma)$) marked on the panels and summarize in Table S1.

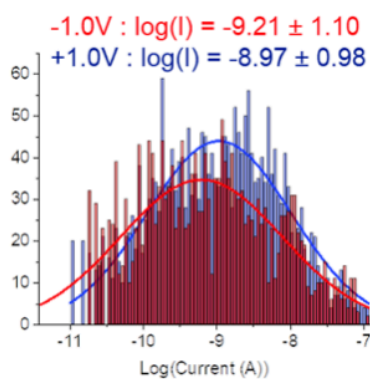
(a) $\text{TSAu-C6/KP}_5\text{W}_{30}\text{//Pt}$



(b) $\text{TSAu-C6/NH}_4\text{P}_5\text{W}_{30}\text{//Pt}$



(c) $\text{TSAu-C6/HP}_5\text{W}_{30}\text{//Pt}$



(d) $\text{TSAu-C6/TBAP}_5\text{W}_{30}\text{//Pt}$

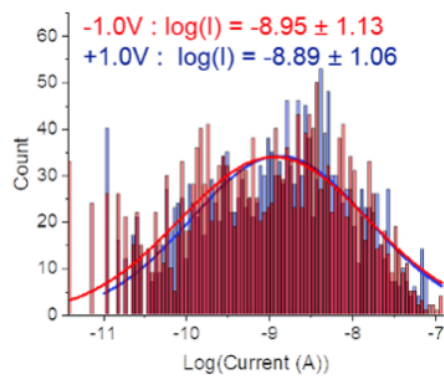


Figure S10. Histograms of $\log(\text{current})$ measured at 1V and -1V for the four samples. The solid lines are the fit by a log-normal distribution with the values of the log-mean ($\log(\bar{I})$) and a log standard deviation ($\log(\sigma)$) marked on the panels and summarize in Table S1.

		KP ₅ W ₃₀	NH ₄ P ₅ W ₃₀	HP ₅ W ₃₀	TBAP ₅ W ₃₀
+0.5 V	log-\bar{I}	-11.18	-10.24	-9.75	-9.35
	\bar{I} (A)	6.6x10 ⁻¹²	5.7x10 ⁻¹¹	1.8x10 ⁻¹⁰	4.5x10 ⁻¹⁰
	log-σ	0.71	0.76	1.03	1.0
-0.5 V	log-\bar{I}	-11.13	-10.24	-9.77	-9.4
	\bar{I} (A)	7.4x10 ⁻¹²	5.7x10 ⁻¹¹	1.7x10 ⁻¹⁰	4.0x10 ⁻¹⁰
	log-σ	0.65	0.78	1.13	1.0
+1 V	log-\bar{I}	-9.89	-9.00	-8.97	-8.89
	\bar{I} (A)	1.3x10 ⁻¹⁰	1.0x10 ⁻⁹	1.1x10 ⁻⁹	1.3x10 ⁻⁹
	log-σ	0.77	0.84	0.98	1.06
-1 V	log-\bar{I}	-9.73	-9.50	-9.21	-8.95
	\bar{I} (A)	1.9x10 ⁻¹⁰	3.2x10 ⁻¹⁰	6.2x10 ⁻¹⁰	1.1x10 ⁻⁹
	log-σ	0.83	0.92	1.10	1.13

Table S1. Values of log-mean ($\log\bar{I}$), mean current \bar{I} , and a log standard deviation ($\log\sigma$) of the current dispersion (log-normal distribution) shown in Fig. S10.

6. Single Energy-Level Model

The single-energy level (SEL) model (Eq. 1 main text), considers that: i) a single molecular orbital (MO) dominates the charge transport, ii) the voltage mainly drops at the molecule/electrode interface and iii) that the MO broadening is described by a Lorentzian or Breit-Wigner distribution.^{16, 17} The simple energy scheme (Fig. S11) is described by ϵ_0 the energy of the MO involved in the transport (with respect to the Fermi energy of the electrodes), Γ_1 and Γ_2 the electronic coupling energy between the MO and the electron clouds in the two electrodes, e the elementary electron charge, h the Planck constant and N the number of molecules contributing to the ET in the molecular junction (assuming independent molecules conducting in parallel, *i.e.* no intermolecular interaction¹⁸⁻²⁰). Albeit this number can be estimated using mechanical models of

the tip/SAM interface in some cases when the Young modulus of the SAM is reasonably known,^{14, 15, 21-23} this is not the case here for the POM/alkyl SAM system for which the Young modulus has not been determined. Consequently, we use $N=1$ throughout this work. This means that the Γ_1 and Γ_2 values are "effective" coupling energies of the SAM with the electrodes and they are used only for a relative comparison of the POM SAMs measured with the same C-AFM conditions in the present work and they cannot be used for a direct comparison with other reported data (as for example from single molecule experiments). We also note that the exact value of N has no significant influence on the fitted parameter ϵ_0 . The fits were done with the routine included in ORIGIN software,²⁴ using the method of least squares and the Levenberg Marquardt iteration algorithm.

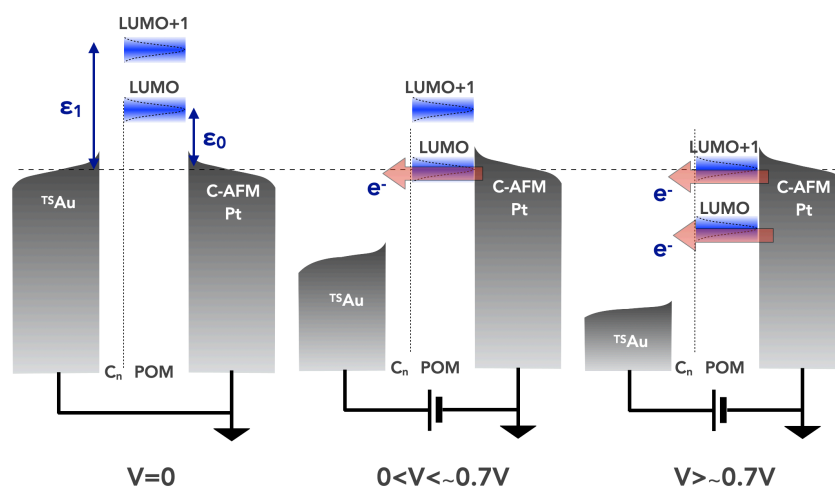


Figure S11. Schematic energy diagram of the molecular junction at 0V, at a moderate positive voltage applied on the Au substrate $V < 0.6-0.7$ V and at higher voltages $V > 0.7$ V.

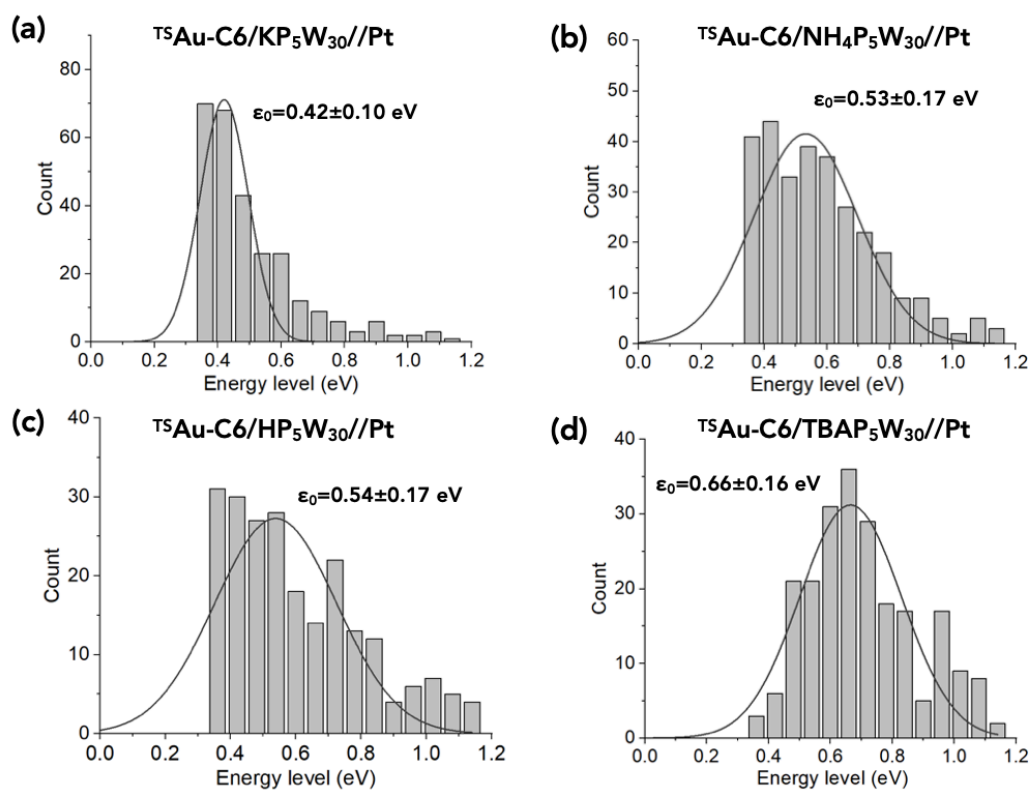


Figure S12. Histograms of the energy values ϵ_0 deduced from the fit of the SEL model on the complete I-V dataset shown in Fig. 2 (main text). The solid lines are the fits by a normal distribution, the mean values are shown in the panels.

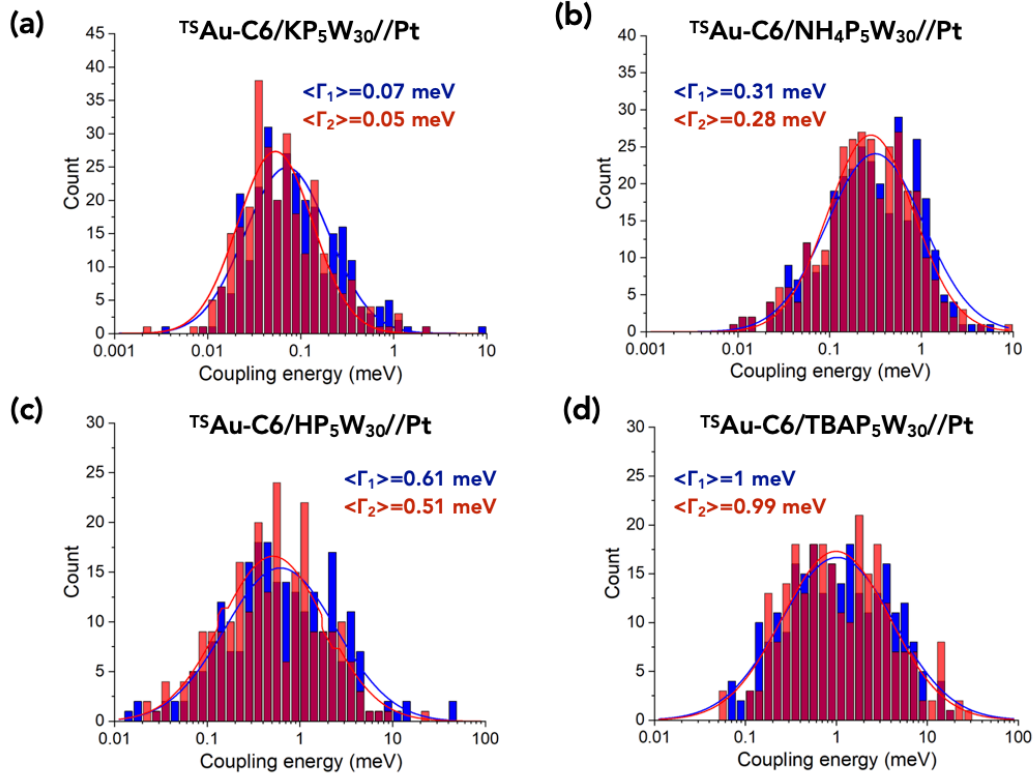


Figure S13. Histograms of the coupling energy values Γ_1 and Γ_2 deduced from the fit of the SEL model on the complete I-V dataset shown in Fig. 2 (main text). The solid lines are the fits by a log-normal distribution, the mean values are shown in the panels.

7. Transition Voltage Spectroscopy

We also used the transition voltage spectroscopy (TVS)²⁵⁻²⁹ to analyze the I-V curves. Plotting $|V^2/I|$ vs. V (Fig. S14),³⁰ we determine the transition voltages V_{T+} and V_{T-} for both voltage polarities at which the bell-shaped curve is maximum. This threshold voltage indicates the transition between off resonant (below V_T) and resonant (above V_T) transport regime in the molecular junctions and can therefore be used to estimate the location of the energy level. In Fig. S14, the thresholds V_{T+} and V_{T-} are indicated by the vertical arrows (with values) and determined from the max of a 2nd order polynomial function fitted around the

max of the bell-shaped curves (to cope with noisy curves). The value of $\epsilon_{0-TV\text{S}}$ is estimated by:²⁷

$$|\epsilon_{0-TV\text{S}}| = 2 \frac{e|V_{T+} V_{T-}|}{\sqrt{V_{T+}^2 + 10|V_{T+} V_{T-}|/3 + V_{T-}^2}} \quad (2)$$

We also determined an average value of the electrode coupling energy $\Gamma_{TV\text{S}}$ using this relationship:^{31, 32}

$$G(0) = N G_0 \frac{\Gamma_{TV\text{S}}^2}{\epsilon_{0-TV\text{S}}^2} \quad (3)$$

with $G(0)$ the zero-bias conductance (Fig. S15), G_0 the conductance quantum ($2e^2/h=7.75 \times 10^{-5}$ S, e the electron charge, h the Planck constant) and N the number of molecules in the junction. G is calculated from the slope of the I-V curve in its ohmic region (-50 mV/50 mV) and $N=1$ (see above). Note that $\Gamma_{TV\text{S}}$ is equivalent to the geometrical average of the SEL values $(\Gamma_1 \Gamma_2)^{1/2}$.^{31, 32}

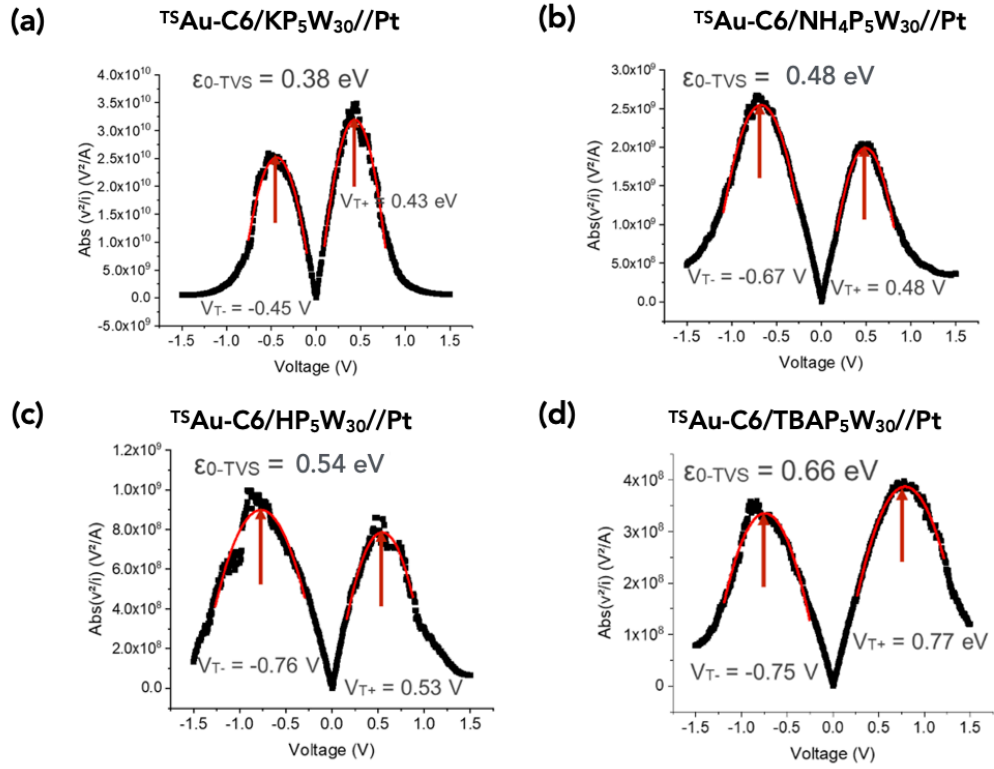


Figure S14. TVS plot from the mean \bar{I} - V traces (Fig. 2 in main text) for the four molecular junctions.

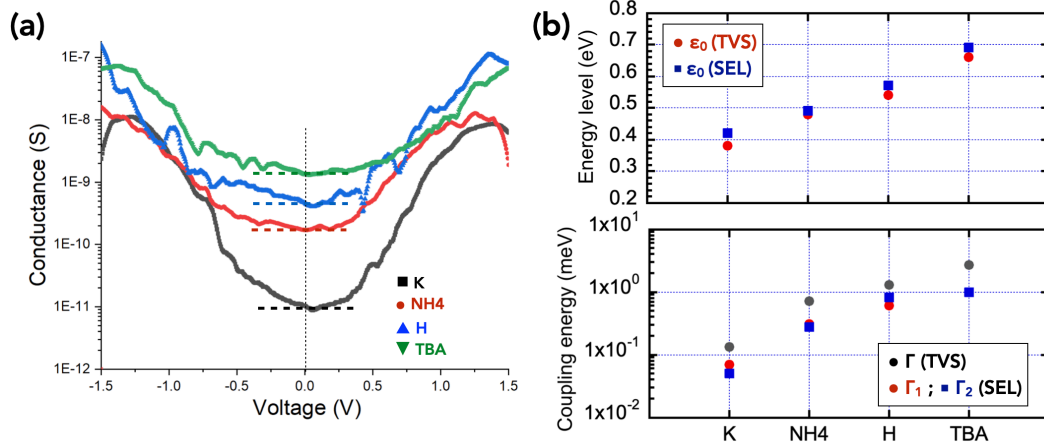


Figure S15. (a) First derivative (with Savitzky–Golay smooth on 20 data points) of the mean \bar{I} - V to determine the zero-bias conductance (horizontal dashed lines)

and (b) comparison of the energy level and electrode coupling energies determined by the SEL model fit and the TVS method.

8. Supplementary figures for discussion

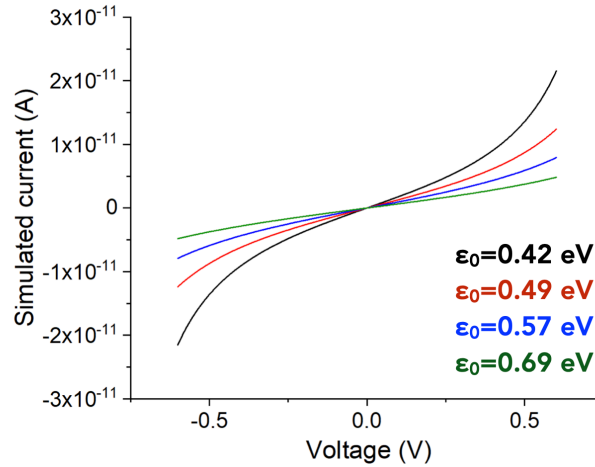


Figure S16. Simulated I - V (Eq. (1) in main text) with ϵ_0 ranging from 0.42 et 0.69 eV (see Table 2, main text) and keeping $\Gamma_1 = \Gamma_2 = 0.1$ meV, $N=1$. The ratio of the currents at ± 0.6 V between the two extreme curves is 4.48.

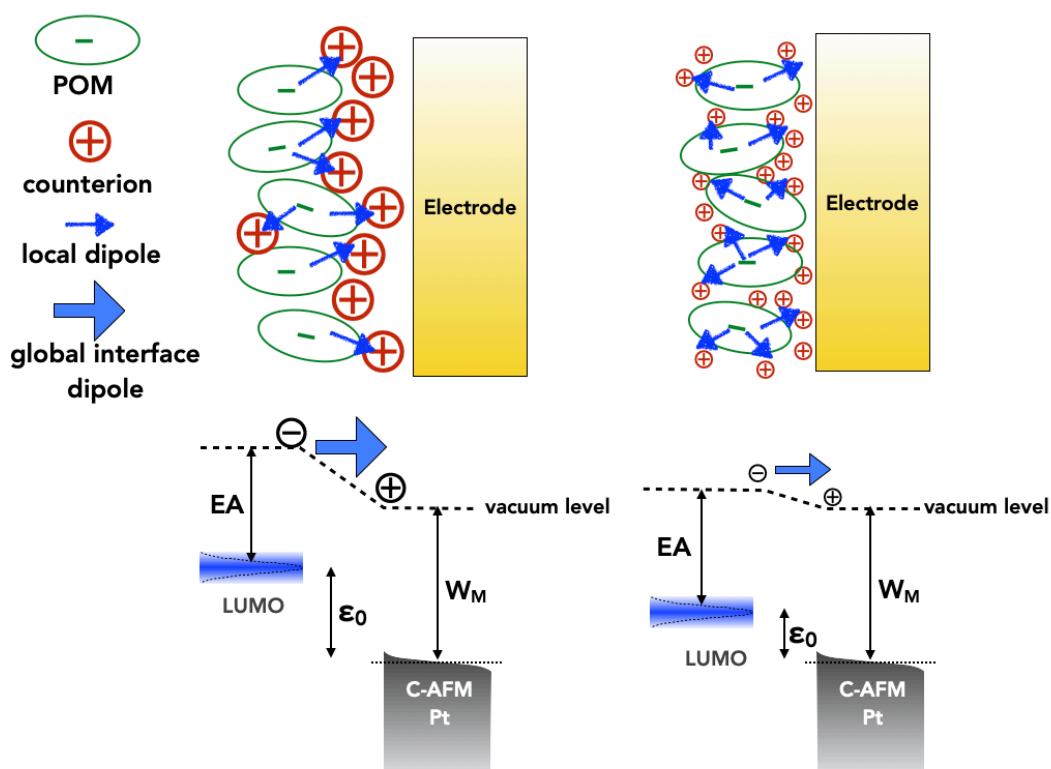


Figure S17. Scheme of two possible scenarios at the POM/electrode interface for the TBA⁺ counterions (left) and the smaller counterions, e.g. H⁺, K⁺ (right). The small blue arrows represent the local dipole between the POM and one counterion (not all represented for clarity). The large blue arrows indicate the resulting global interface dipoles that induce a vacuum level shift. For simplicity, we assume the same metal work function (W_M) and molecule electron affinity (EA) in the two cases. Due to the dipole-induced vacuum level shift, the LUMO is shifted upwards for the TBA⁺ scenario (larger ϵ_0).

9. Two-sample t-test

To determine if the small current asymmetry at +1V and -1V for the HP₅W₃₀ and NH₄P₅W₃₀ is statistically significant, we performed a two-sample t-test using the routine provided by ORIGIN software.²⁴ Since the t-test applies for normally distributed populations and the currents are log-normal distributed (Fig. S10), we

consider the decimal logarithm of the currents taken from the datasets shown in Fig. 2 (main text) at -1V and +1V as the two populations 1 and 2 (P1, P2). We test the null hypothesis that the mean values are equal, $\text{mean}(P1) - \text{mean}(P2) = 0$. At a significance level of 0.05, the data yielded a probability p-value that the null hypothesis is true of 4×10^{-9} for HP_5W_{30} and 6×10^{-12} for $\text{NH}_4\text{P}_5\text{W}_{30}$, which are less than our 0.05 significance level, and thus we can reject the null hypothesis. In other words, the weak current asymmetry can be considered as statistically significant.

References

- (1) Creaser, I.; Heckel, M. C.; Neitz, R. J.; Pope, M. T. Rigid nonlabile polyoxometalate cryptates $[\text{ZP}_5\text{W}_3\text{O}_{110}](15-n)$ - that exhibit unprecedented selectivity for certain lanthanide and other multivalent cations. *Inorganic Chemistry* **1993**, 32 (9), 1573-1578.
- (2) Jeannin, Y.; Martin-Frere, J.; Choi, D. J.; Pope, M. T. The Sodium Pentaphosphato(V)-Triacontatungstate Anion Isolated as the Ammonium Salt. In *Inorganic Syntheses*, Ginsberg, A. P. Ed.; Vol. 27; Wiley & son, 1990; pp 115-118.
- (3) Sadakane, M.; Ichi, Y.; Ide, Y.; Sano, T. Thermal Stability and Acidic Strength of Preyssler-Type Phosphotungstic Acid, $\text{H}_{14}[\text{P}_5\text{W}_3\text{O}_{110}\text{Na}]$ and Its Catalytic Activity for Hydrolysis of Alkyl Acetates. *Zeitschrift für anorganische und allgemeine Chemie* **2011**, 637 (14-15), 2120-2124.
- (4) Sapiro, K.; Kawato, Y.; Koike, K.; Sano, T.; Nakai, T.; Sadakane, M. Preyssler-type phosphotungstate is a new family of negative-staining reagents for the TEM observation of viruses. *Scientific Reports* **2022**, 12 (1), 7554.
- (5) Contant, R.; Klemperer, W. G.; Yaghi, O. Potassium Octadecatungstodiphosphates(V) and Related Lacunary Compounds. In *Inorganic Syntheses*, Ginsberg, A. P. Ed.; Wiley and son, 1990; pp 104-111.
- (6) Cantwell, F. F.; Nielsen, J. S.; Hrudey, S. E. Free nickel ion concentration in sewage by an ion exchange column-equilibration method. *Analytical Chemistry* **1982**, 54 (9), 1498-1503.
- (7) Hegner, M.; Wagner, P.; Semenza, G. Ultralarge atomically flat template-stripped Au surfaces for scanning probe microscopy. *Surf. Sci.* **1993**, 291, 39-46.

- (8) Weiss, E.; Chiechi, R.; Kaufman, G.; Kriebel, J.; Li, Z.; Duati, M.; Rampi, M.; Whitesides, G. Influence of defects on the electrical characteristics of mercury-drop junctions: self-assembled monolayers of n-alkanethiolates on rough and smooth silver. *J. Am. Chem. Soc.* **2007**, *129* (14), 4336-4349.
- (9) Weiss, E. A.; Kaufman, G. K.; Kriebel, J. K.; Li, Z.; Schalek, R.; Whitesides, G. M. Si/SiO₂-Templated Formation of Ultraflat Metal Surfaces on Glass, Polymer, and Solder Supports: Their Use as Substrates for Self-Assembled Monolayers. *Langmuir* **2007**, *23* (19), 9686-9694.
- (10) Dalla Francesca, K.; Lenfant, S.; Laurans, M.; Volatron, F.; Izzet, G.; Humblot, V.; Methivier, C.; Guerin, D.; Proust, A.; Vuillaume, D. Charge transport through redox active [H7P8W48O184](33-) polyoxometalates self-assembled onto gold surfaces and gold nanodots. *Nanoscale* **2019**, *11* (4), 1863-1878.
- (11) Huez, C.; Guérin, D.; Lenfant, S.; Volatron, F.; Calame, M.; Perrin, M. L.; Proust, A.; Vuillaume, D. Redox-controlled conductance of polyoxometalate molecular junctions. *Nanoscale* **2022**, (14), 13790.
- (12) Ulman, A. *An introduction to ultrathin organic films : from Langmuir-Blodgett to Self-assembly*; Academic press, 1991.
- (13) Rabe, J. P.; Knoll, W. An ellipsometric method for the characterization of macroscopically heterogeneous films. *Optics Communications* **1986**, *57* (3), 189-192.
- (14) Engelkes, V. B.; Daniel Frisbie, C. Simultaneous nanoindentation and electron tunneling through alkanethiol self-assembled monolayers. *The Journal of Physical Chemistry B* **2006**, *110* (20), 10011-10020.
- (15) Smaali, K.; Desbief, S.; Foti, G.; Frederiksen, T.; Sanchez-Portal, D.; Arnau, A.; Nys, J. P.; Leclere, P.; Vuillaume, D.; Clement, N. On the mechanical and electronic properties of thiolated gold nanocrystals. *Nanoscale* **2015**, *7* (5), 1809-1819.
- (16) Datta, S. *Electronic transport in mesoscopic systems*; Cambridge University Press, 1995.
- (17) Cuevas, J. C.; Scheer, E. *Molecular Electronics: An introduction to theory and experiment*; World Scientific, 2010.
- (18) Magoga, M.; Joachim, C. Conductance of molecular wires connected or bonded in parallel. *Phys. Rev. B* **1999**, *59*, 16011-16021.
- (19) Reuter, M. G.; Hersam, M. C.; Seideman, T.; Ratner, M. A. Signatures of Cooperative Effects and Transport Mechanisms in Conductance Histograms. *Nano Letters* **2012**, *12* (5), 2243-2248.

- (20) Trasobares, J.; Rech, J.; Jonckheere, T.; Martin, T.; Aleveque, O.; Levillain, E.; Diez-Cabanes, V.; Olivier, Y.; Cornil, J.; Nys, J. P.; et al. Estimation of π - π Electronic Couplings from Current Measurements. *Nano Letters* **2017**, *17* (5), 3215–3224.
- (21) Cui, X. D.; Primak, A.; Zarate, X.; Tomfohr, J.; Sankey, O. F.; Moore, A. L.; Moore, T. A.; Gust, D.; Harris, G.; Lindsay, S. M. Reproducible measurement of single-molecule conductivity. *Science* **2001**, *294*, 571-574.
- (22) Cui, X. D.; Zarate, X.; Tomfohr, J.; Sankey, O. F.; Primak, A.; Moore, A. L.; Moore, T. A.; Gust, D.; Harris, G.; Lindsay, S. M. Making electrical contacts to molecular monolayers. *Nanotechnology* **2002**, *13*, 5-14.
- (23) Morita, T.; Lindsay, S. Determination of Single Molecule Conductances of Alkanedithiols by Conducting-Atomic Force Microscopy with Large Gold Nanoparticles. *J Am Chem Soc* **2007**, *129* (23), 7262-7263.
- (24) *ORIGIN, version 2019*; OriginLab Corporation, Northampton, MA, USA.
- (25) Beebe, J. M.; Kim, B.; Gadzuk, J. W.; Frisbie, C. D.; Kushmerick, J. G. Transition from Direct Tunneling to Field Emission in Metal-Molecule-Metal Junctions. *PHYSICAL REVIEW LETTERS* **2006**, *97* (2), 026801.
- (26) Beebe, J. M.; Kim, B.; Frisbie, C. D.; Kushmerick, J. G. Measuring Relative Barrier Heights in Molecular Electronic Junctions with Transition Voltage Spectroscopy. *ACS Nano* **2008**, *2* (5), 827-832.
- (27) Bâldea, I. Ambipolar transition voltage spectroscopy: Analytical results and experimental agreement. *Physical Review B* **2012**, *85* (3), 035442.
- (28) Huisman, E. H.; Guédon, C. M.; van Wees, B. J.; van der Molen, S. J. Interpretation of Transition Voltage Spectroscopy. *Nano Lett* **2009**, *9* (11), 3909-3913.
- (29) Mirjani, F.; Thijssen, J. M.; van der Molen, S. J. Advantages and limitations of transition voltage spectroscopy: A theoretical analysis. *Physical Review B* **2011**, *84* (11), 115402.
- (30) Bâldea, I. Important issues facing model-based approaches to tunneling transport in molecular junctions. *Physical Chemistry Chemical Physics* **2015**, *17* (31), 20217-20230.
- (31) Bâldea, I. Transition voltage spectroscopy reveals significant solvent effects on molecular transport and settles an important issue in bipyridine-based junctions. *Nanoscale* **2013**, *5* (19), 9222-9230.
- (32) Xie, Z.; Bâldea, I.; Frisbie, C. D. Energy Level Alignment in Molecular Tunnel Junctions by Transport and Spectroscopy: Self-Consistency for the Case of Alkyl Thiols and Dithiols on Ag, Au, and Pt Electrodes. *J Am Chem Soc* **2019**, *141* (45), 18182-18192.